This is the Pre-Published Version.

S. Lin, T. Chow, X. Huang (2021) *Smoldering Propagation and Blow-off on Consolidated Fuel under External Airflow*, **Combustion and Flame**, 234, 111685. https://doi.org/10.1016/j.combustflame.2021.111685

Smoldering Propagation and Blow-off on Consolidated Fuel under External Airflow

Shaorun Lin[1,2], Tsz Him Chow[1], and Xinyan Huang[1,*]

[1]*Research Centre for Fire Safety Engineering, The Hong Kong Polytechnic University, Kowloon, Hong Kong SAR*

[2]*The Hong Kong Polytechnic University Shenzhen Research Institute, Shenzhen, Guangdong, China*

*Corresponding to xy.huang@polyu.edu.hk (X. Huang)

Abstract

The propagation of smoldering combustion and the blow-off limit are of practical importance in evaluating the fire dynamics of solid fuels, but the scientific understanding is still limited. In this work, we quantify the smoldering propagation rate on consolidated biomass and the blow-off limit under concurrent and opposed external airflows up to 50 m/s. The incense cylinders with different diameters (1.5-5 mm) and densities (720-1,100 kg/m^3) are tested. As the airflow velocity increases, the smoldering propagation rate first increases to its maximum value (Oxygen-limited Regime) and subsequently remains stable (Thermal Regime), regardless of the airflow direction. Afterward, it slightly decreases (Chemical Regime) until blow-off, and the blow-off of opposed smoldering is easier, similar to the pattern of flame spread. The blow-off airflow velocity (13-46 m/s) of smoldering combustion is around ten times larger than that of flaming combustion, and it decreases as the fuel diameter or density increases. This work advances the fundamental understanding of the smoldering propagation, blow-off, and its persistence; thus, helping guide the fire suppression strategies of smoldering.

Keywords: *smoldering fire; extinction limit; oxygen supply; biomass; wind effect.*

1. Introduction

Smoldering is the slow, low-temperature, and flameless burning of porous fuels and one of the most persistent types of combustion phenomena [1–3]. Smoldering combustion is a heterogeneous process sustained when oxygen directly attacks the hot fuel surface, different from the flame regarding the combustion chemistry and transport processes [2,3]. Smoldering can be ignited easily by a weak heat source [2–4] or even self-ignited, which usually occur in silos and large fuel piles [5], creating a shortcut to more intensive flaming fires (through smoldering-to-flaming transition). Moreover, it is also challenging to detect and suppress the hidden smoldering fire. For example, the colossal piles of World Trade Center debris continued to smolder for more than half a year, despite substantial firefighting operations [6]. Natural smoldering, such as the underground fires in peatlands or coal mines, is one of the most extensive and longest-lasting fire phenomena on Earth [7,8]. Therefore, it is vital to deepen our understanding of smoldering fire dynamics.

Nomenclature

Symbols		***Greeks***	
a	strain rate (s^{-1})	α	thermal diffusivity (m^2/s)
c	specific heat capacity (J/kg-K)	δ	thickness (m)
d	fuel diameter (mm)	ν	stochiometric coefficient (-)
C	fitting coefficient (-) / constant (-)	υ	kinematic viscosity (m^2/s)
D	wind tunnel diameter (m)	ρ	density (kg/m^3)
Da	Damkohler number (-)	λ	thermal conductivity (W/m-K)
h	convection coefficient (W/m^2-K)	ϕ	porosity (-)
h_m	mass transfer coefficient (kg/m^2-s)	$\dot{\omega}$	reaction rate (1/s)
Δh	thermal enthalpy difference (J/kg)		
ΔH_c	heat of combustion (MJ/kg)		
I	thermal inertia (J/m^2-K-$s^{1/2}$)	***Subscripts***	
k	permeability (m^2)	a	airflow/ambient
L	length (m)	ch	chemical
$\dot{m}''$	mass flux (kg/m^2-s)	con	concurrent
ΔP	pressure difference (Pa)	$cond$	conduction
$\dot{q}''$	heat flux (kW/m^2)	$conv$	convection
$\dot{R}$	regression rate (m/s)	ex	extinction
Re	Reynolds number (-)	f	fire
Δt	time (s)	F	fuel
T	temperature (K)	o	initial
u_a	internal airflow velocity (m/s)	ox	oxygen
U_a	external airflow velocity (m/s)	p	preheating
V	fire propagation rate (cm/min)	r	residence
Δx	distance (m)	sm	smoldering
Y	mass fraction (%)	T	thermal

The fire spread (propagation) process is of practical significance in evaluating the impact of fire events [9–12]. The fire spread is a continuous ignition and burning process [13], depending on both environment (e.g., wind [10,11,14–16], oxygen [17–19], pressure [20,21], temperature [22,23], and gravity [24]) and fuel factors (e.g., type/array [25], moisture [16], density [26], orientation [27], and size [28,29]). Based on the relative direction to the airflow (or wind), fire spread can be classified into the concurrent and opposed modes [9–11]. In the literature, most studies have focused on the characteristics of flame spread on solid fuels [9–11,30], rather than the smoldering spread.

Smoldering combustion is controlled by the competition between the oxygen supply and the heat transfer to and from the reaction zone [3,31,32]. Therefore, the airflow or wind is crucial to smoldering propagation, because it could increase both the oxygen supply and the heat loss [15,29,33]. By applying an external airflow (or environmental wind), smoldering propagation may become faster because of the increased oxygen supply (O_2-limit regime) [1,11,17]. Afterward, the excessive airflow may also help

trigger gas-phase homogenous oxidation under some specific conditions and result in smoldering-to-flaming (StF) transition [19,34]. However, for flaming fires, flame spread increases with wind speed due to increased convective heating on the unburnt fuel, rather than increased oxygen supply [33]. On the other hand, the porosity and permeability of fuel also affect the oxidation-controlled smoldering processes. For high-permeability fuels, such as cotton [15,35], pine needle [36], and PU foam [37], oxygen can diffuse into the porous fuel to maintain an internal smoldering propagation. For low-permeability consolidated fuels like wood [38], fiberboard [1], and coal chunk [8], smoldering can only propagate from outside to inside like a regression process, because oxygen could only diffuse through the porous char that is produced from the first-stage pyrolysis process [11]. Further increasing the airflow velocity, the cooling effect becomes dominant, so eventually, smoldering extinction or blow-off will occur, just like the blow-off of flame [39].

In the literature, the blow-off of flame on solid fuels has been extensively studied over the last 50 years [4,11]. For example, Loh and Fernandez-Pello [40] showed that the concurrent rate flame spread over the thin paper first increased with the airflow velocity (< 1 m/s) but became almost constant until blow-off at about 3 m/s. A similar trend and blow-off wind speed were also observed for the concurrent flame spread on thin electrical wires [41]. In general, the blow-off of opposed flame spread is easier, usually at an airflow velocity lower than 1 m/s [42,43]. Comparatively, the research on the blow-off of smoldering is limited; and generally, it is more difficult to blow off persistent smoldering fire. Palmer [1] found that the blow-off limit of opposed smoldering propagation over fiberboard was about 7 m/s, but the concurrent smoldering propagation could still be sustained at 10 m/s [1,11]. Like the flame, most smoldering extinction processes result from a local energy imbalance, where the cooling rate is larger than the heat-release rate from exothermic oxidations [4,39,44]. Thus, decreasing oxygen concentration and pressure promotes the blow-off of smoldering under a smaller airflow [19,20]. So far, no study has addressed the smoldering propagation at large wind speeds over 10 m/s and the blow-off limits of persistent smoldering fire; thus, there is a big knowledge gap.

This work investigated both concurrent and opposed smoldering propagations over cylindrical consolidated biomasses (incenses) with different fuel diameters (1.5-5 mm) and densities (720-1,100 kg/m^3). The external airflow velocity of up to 50 m/s in a small wind tunnel was applied to explore the blow-off limits. The theoretical analysis was proposed to explain the influence of environmental and fuel properties on smoldering propagation and critical conditions of blow-off.

2. Experimental Methods

2.1. Materials

The cylindrical consolidated rod (i.e., incense), a representative biomass fuel that is prone to smoldering combustion, was tested in this work (Fig. 1a). The incense is an aromatic biotic material that is widely used in cultural and religious events in Asia. It mainly consists of mixed wood dust from the aromatic plants (e.g., from sage and cedar) and has homogenous porosity and composition [45]. The

thermal analysis (TGA-DSC) of this incense was conducted, and the data is shown in Fig. A1 of the Appendix. The details of the front and cross-section of the incense are also shown in Fig. 1a. Unlike the cotton bales and plastic foams, the dust particles inside the incense are densely packed, so oxygen is difficult to flow or diffuse into its internal structure.

Before the test, the incenses were first oven-dried at 75 ºC for at least 48 h. Afterward, all samples were placed into an electronic dry cabinet to avoid the re-absorbing of moisture from the air. To explore the effect of fuel diameter (d) and density (ρ) on the smoldering propagation, two groups of experiments were designed:

(I) three sample diameters of 1.5, 2.5, and 5.0 mm with a constant fuel density of 720 kg/m^3, and

(II) three sample densities of 720, 920, and 1,100 kg/m^3 with a constant diameter of 1.5 mm.

To help estimate the rate of smoldering propagation, the long incense rod was cut into 10-15 cm samples and marked like a ruler with an interval of 1 cm (see Fig. 1a).

2.2. Environmental control

The experiments of smoldering propagation and blow-off under external airflow were conducted inside a small wind tunnel. The customized tubular wind tunnel was made of quartz glass and had an inner diameter (D) of 2 cm and a length of 20 cm, as illustrated in Fig. 1(b). The airflow (20.9% oxygen) from the compressed tank was fed through the bottom of the quartz glass tube, and then homogenized through a layer of small steel beads. A similar setup was used previously to study the flame spread [24] and smoldering propagation [19] under opposed flow with different oxygen mass fractions. Before the test, the airflow velocity (U_a up to 50 m/s) was controlled and measured by a precision anemometer.

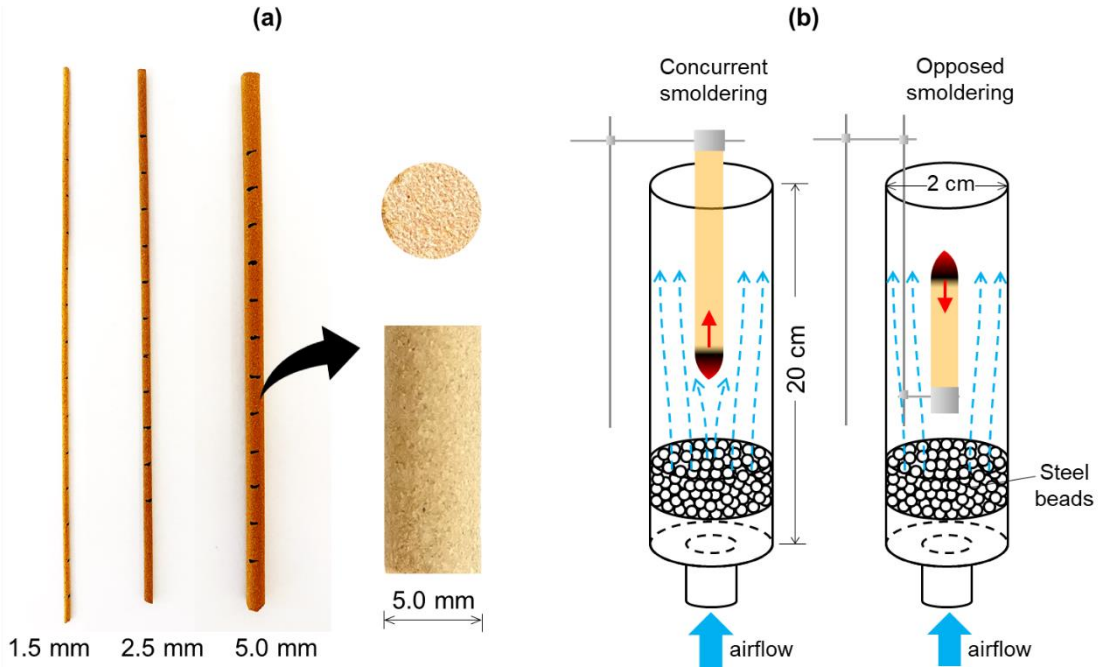

Fig. 1. (a) Photos of cylindrical incenses with different diameters with enlarged details of surface and cross-section, and (b) schematic of experimental setups for concurrent and opposed smoldering propagation under external airflow.

For an internal flow in a circular tube of diameter D, the Reynolds number (Re_D) can be calculated as $Re_D = U_a D/\upsilon$, where $\upsilon \approx 16 \times 10^{-6}$ m^2/s is the kinematic viscosity of the air at ambient temperature [46]. In other words, when the airflow velocity is larger than 2 m/s, the mainstream flow inside the tube is turbulent (Re_D> 2,300) where its velocity profile is relatively flat. Because the inlet flow is disturbed through a long gas pipeline and a layer of steel bead, it is expected that the downstream flow through the tube is quite turbulent. On the other hand, the Reynolds number for the external airflow over the fuel surface ($Re_F = U_a d/\upsilon$) is much smaller than the turbulent limit of 5×10^5, so the boundary-layer flow on the fuel surface is laminar.

2.3. Test procedure

The biomass sample was ignited by a torch at one end, and then inserted into the middle part of the wind tunnel and fixed vertically at the tube axis by a sample holder, as shown in Fig. 1(b). The ignited end (~5 mm) was placed on the bottom for the concurrent smoldering propagation, while for the opposed propagation, the ignited end was on the top. To reduce the effect of ignition, the smoldering front was allowed to propagate 20-30 mm away from the ignition region before calculating the smoldering propagation rate. Afterward, wind with prescribed speed was applied, and shortly after, the smoldering propagation reached the quasi-steady state (see more details in Fig. A2 in Appendix). The external wind was applied in a step-increase manner from no wind (i.e., $U_a \approx 0$ as the base case) until the critical airflow velocity for blow-off (U_{ex}) was found. To start a new test under a different wind velocity, a fresh fuel sample was used.

A side-view digital video camera was used to capture the time history of the smoldering front. Through image analysis frame by frame, the instantaneous smoldering propagation rate (V_{sm}) can be calculated as $V_{sm} = \Delta x/\Delta t$, where Δt is the required duration for a smoldering front to propagate for a certain distance of Δx. Then, we could judge whether a steady-state propagation was reached (see Fig. A2 in the Appendix). For each scenario, tests were repeated at least three times to quantify the standard deviations, and more repeating tests were conducted near the blow-off limit. In general, good experimental repeatability was found. During the tests, the ambient temperature (T_a) was 23 ± 2 ºC, and the relative humidity was 50 ± 10%.

3. Results and Discussion

3.1. Smoldering phenomena

Fig. 2(a) and (b) shows some typical photos of concurrent and opposed smoldering propagation under different airflow velocities of 0, 5, and 10 m/s with fuel diameters of 1.5, 2.5, and 5.0 mm. As the wind velocity increased, the smoldering of incense was stronger due to a better oxygen supply, where the conical reaction surface was hot enough to emit visible light (glowing incandescence) [11]. However, no smoldering-to-flaming transition was observed in this work, different from the past low-airflow tests [19–21]. This was probably because the external wind was already large enough to blow

off the flame (usually < 5 m/s [40–43]). On the other hand, except for oxygen supply, the permeability of a fuel and its ability to remain consolidated may also affect this transition [33]. Nevertheless, increasing the oxygen concentration could promote the transition to flame in a smaller airflow [34].

Moreover, compared to the opposed propagation, the glowing zone is brighter for the concurrent propagation under the same airflow velocity. The length of the glowing zone (δ_{sm} or smoldering front thickness) increased as the fuel diameter increased, but it was insensitive to the airflow velocity unless near the blow-off limit. The flat leading edge of the glowing region (not the tip of conical shape) was used to track the smoldering front. The glowing tip might not be the perfectly conical shape or clearly observed, because an ash layer sometimes remained and covered the conical tip, just like the burning cigarette (see the supplementary video). Fig. 2(c) also shows a typical blow-off process for the smoldering over a 2.5-mm thick incense, where the opposed airflow velocity was increased to 15 m/s. Gradually, the smoldering (glowing) zone became weaker, flatter, and smaller. After maintaining for about 3 min, the smoldering was eventually blown off.

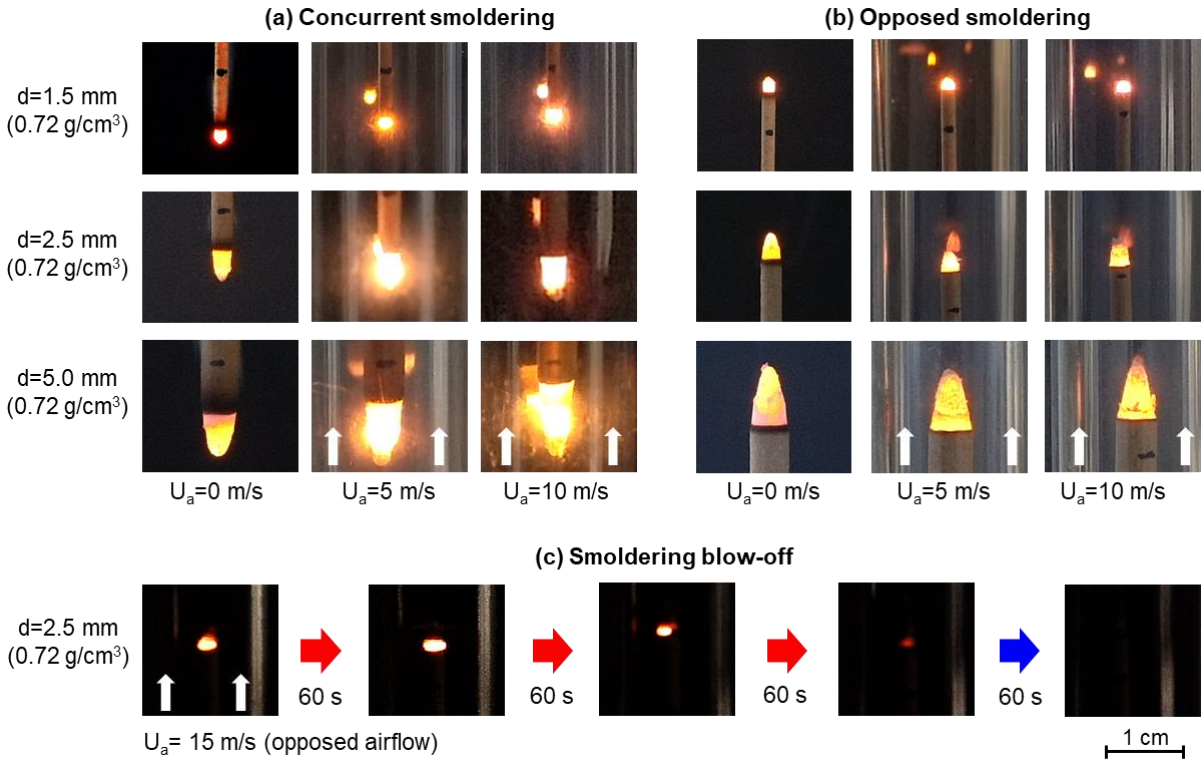

Fig. 2 Smoldering propagation on incense rods of 1.5, 2.5, and 5.0-mm diameters under (a) concurrent, and (b) opposed airflow velocities of 0, 5, and 10 m/s; and (c) blow-off for smoldering on a 2.5-mm incense under the opposed airflow velocity of 15 m/s.

3.2. Smoldering propagation rate vs. airflow direction

Fig. 3 compares the rate of smoldering propagation at different airflow directions. As expected, the concurrent smoldering propagation is much faster than the opposed propagation, and the trend of which is essentially the same as flame spread [11]. For example, for a 2.5-mm thick incense, the

smoldering propagation rate is around 1.9 cm/min under a concurrent airflow of 5 m/s, tripling that under an opposed airflow.

In general, the fire spread can be viewed as a continuous ignition process [9,11]. Thus, its rate is driven by the heat transfer from the oxidation zone ($\dot{q}''$) and resisted by the fuel thermal inertia ($\rho_F \Delta h_F$) [11] as

$$V_{sm} = \frac{\dot{q}'' L_p}{\rho_F \delta_T c_F (T_{sm} - T_a)} \approx \frac{\dot{q}''}{\rho_F \Delta h_F} = \frac{\text{Fire driving force}}{\text{Material resistance}} \quad (1)$$

where ρ_F, c_F, T_{sm}, and $\Delta h_F = c_F(T_{sm} - T_o)$ are the fuel bulk density, specific heat capacity, smoldering temperature, and enthalpy change, respectively. The effect of permeability or porosity (ϕ) could be reflected by the difference in bulk density (ρ_F) as $\rho_F = (1-\phi)\rho_s$, where ρ_s is the solid density of biomass sample. For smoldering fire propagation, the preheated length (L_p) from glowing char-oxidation zone to the unburnt zone is close to the thermal penetration depth (δ_T), i.e., $L_p \approx \delta_T$, because both are the characteristic length of heat conduction in solid fuel [11].

As illustrated in Fig. 3(b), for concurrent smoldering propagation, the airflow can directly attack the conical reaction front, so partial airflow may permeate into the porous glowing zone in the form of a Darcy flow. The excessive oxygen supply intensifies the char oxidation and increases smoldering temperature (see intense incandescence in Fig. 2(a)), so a larger preheating flux ($\dot{q}''$) will be conducted from the reaction front to the preheated zone. In addition, the conical glowing zone may preheat the airflow boundary layer, which can preheat the downstream unburnt fuel via convection. Both effects of the concurrent airflow can speed up the smoldering propagation.

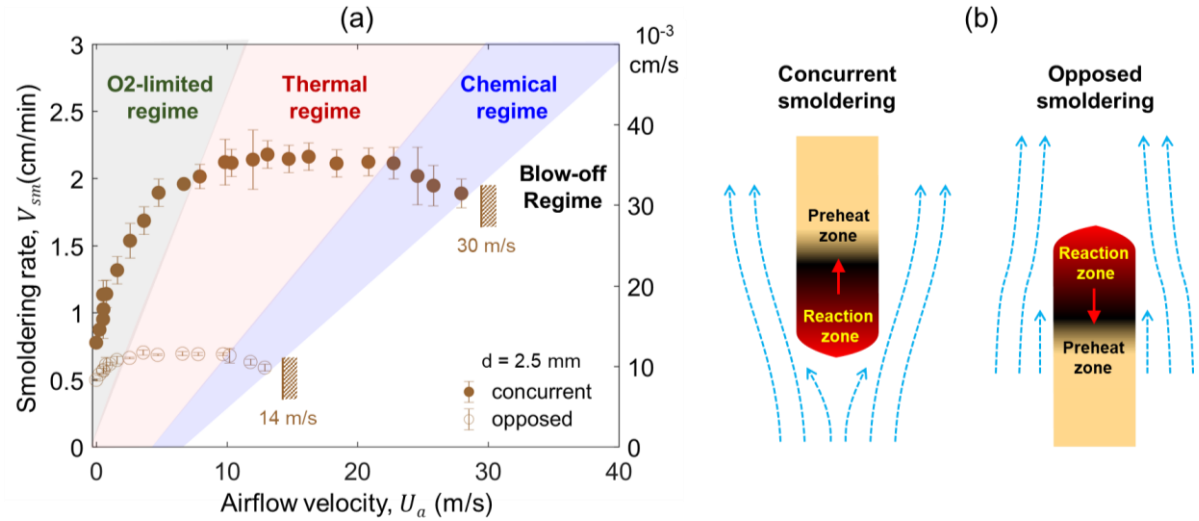

Fig. 3. (a) Comparison of smoldering propagation rate under external concurrent and opposed airflow, where the markers show the average values and error bars show the standard deviations, and (b) schematic diagrams of smoldering propagation under concurrent and opposed airflow.

In contrast, for the smoldering propagation under opposed airflow, the cool airflow can directly cool the unburnt zone, reducing the preheating from the hot glowing zone ($\dot{q}''$) to the preheat zone.

Furthermore, the oxygen can only reach the char surface via diffusion of the boundary layer, rather than the pressure-driven Darcy flow under concurrent airflow. Thus, the oxygen supply from the opposed airflow is less sufficient, slowing down the smoldering propagation. The relatively limited oxygen supply of opposed smoldering is also reflected by a weaker glowing zone in Fig. 2(b).

3.3. Effect of airflow velocity

Fig. 3 also illustrates the effect of airflow velocity on the smoldering propagation rate, where a similar trend is found for both concurrent and opposed propagations (see more comparisons in Figs. 4a-b and 5a-b). That is, as the external airflow velocity increases, the smoldering propagation rate first increases rapidly to the maximum value (O_2-limited Regime) and then remains constant over a wide range of airflow velocities (Thermal Regime). Subsequently, the propagation rate slightly decreases (Chemical Regime) until blow-off, following a similar pattern of concurrent flame spread [41,42].

In a small-airflow regime, the smoldering temperature increases with airflow velocity, indicated by a brighter glowing zone. Therefore, oxygen supply controls the smoldering propagation in this regime, while the cooling effect of airflow is negligible. For example, as the concurrent airflow velocity increases from 0 m/s to 3 m/s, the rate of smoldering propagation on the 2.5-mm thick fuel monotonically increases from 0.8 cm/min to 1.6 cm/min. Such an increasing trend is defined as the O_2-limited Regime, referring to the terminology widely used for the opposed flame spread [11,14,17].

For a consolidated fuel, the smoldering propagation could be regarded as a burning or fuel-regression process, similar to the burning of a candle or the premixed flame [11,15,29]. Therefore, the smoldering propagation rate (V_{sm}) is the same as the regression rate ($\dot{R}$) as

$$V_{sm} = \dot{R} = \frac{\dot{m}_F''}{\rho_F} = \frac{\dot{m}_a''}{v\rho_F} = \frac{\rho_a Y_{ox}}{v\rho_F} u_a \qquad (O_2\text{-limited Regime}) \qquad (2)$$

where u_a is the velocity of internal airflow inside the conical porous char. Its magnitude could be estimated by Darcy's law dominated in the concurrent smoldering and by the diffusion within the boundary layer dominated in the opposed smoldering as

$$u_a = \begin{cases} \dfrac{k}{\phi\mu d}\Delta p = \dfrac{k}{\phi\mu d}\left(\dfrac{1}{2}\rho_a U_a^2\right) \propto \dfrac{U_a^2}{d} & \text{(concurrent)} \\ \dfrac{h_m}{\rho_a} = \dfrac{h}{\rho_a c_p} = Nu\dfrac{\alpha}{d} \propto \dfrac{Re^m}{d} \propto \left(\dfrac{U_a}{d}\right)^m & \text{(opposed)} \end{cases} \qquad (3)$$

where the Nusselt number changes with flow velocity and diameter as $Nu \approx CRe^m Pr^{1/3}$ with $m = 0.5\sim1$. For opposed smoldering propagation, the internal airflow velocity still changes with the external airflow (U_a) but is several orders of magnitude smaller than that of concurrent smoldering propagation. Therefore, the smoldering propagation rate at the O_2-limited Regime increases with the airflow velocity, regardless of the flow direction (see Fig. 3a).

Continuously increasing the airflow velocity, the smoldering propagation rate becomes stable. For example, the concurrent propagation rate on the 2.5-mm thick fuel remains at 2.1 ± 0.3 cm/min from 7 m/s to 23 m/s in Fig. 3(a), regardless of the airflow velocity. In this large-airflow regime, the unlimited oxygen supply no longer affects the smoldering propagation rate. Instead, the thermal conduction within the fuel ($\dot{q}'' \approx \lambda_F(T_{sm} - T_o)/\delta_T$) starts to dominate the smoldering propagation [11]. This behavior is similar to the Thermal Regime of the flame spread, where the preheating of flame controls the rate of flame spread [42,47]. Based on Eq. (1), the smoldering propagation rate at the Thermal Regime is free of oxygen effect and reach the maximum value as

$$V_{sm} = V_{max} = \frac{\dot{q}''}{\rho_F c_F (T_{sm} - T_o)} = \frac{\lambda_F (T_{sm} - T_o)/\delta_T}{\rho_F c_F (T_{sm} - T_o)} \approx \frac{\alpha_F}{\delta_T} \quad \text{(Thermal Regime)} \quad (4)$$

where λ_F and α_F are the fuel thermal conductivity and diffusivity, and δ_T is the thermal length within the fuel. Therefore, the Thermal-Regime smoldering propagation rate is insensitive to the external airflow velocity.

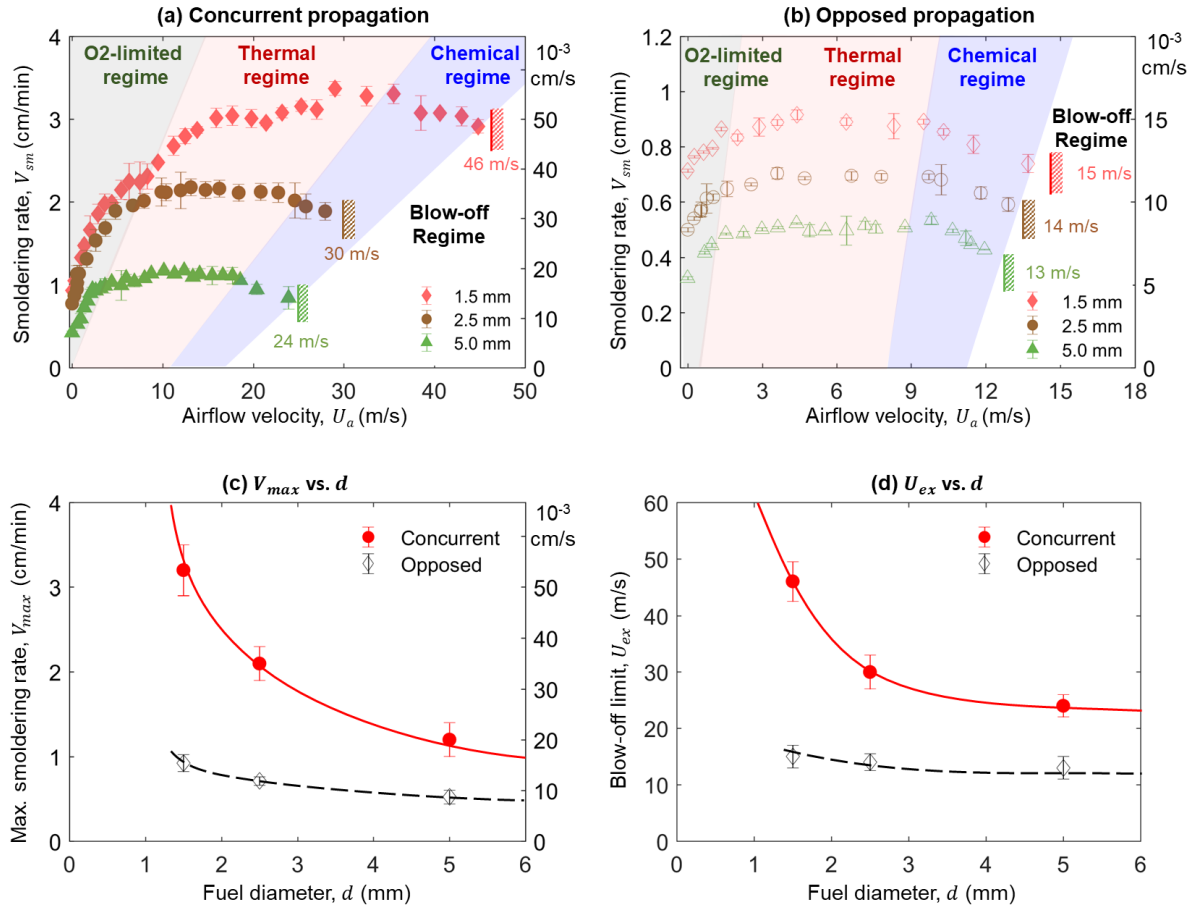

Fig. 4 Effect of fuel diameter on the rate of smoldering propagation under (a) concurrent and (b) opposed airflow, (c) maximum smoldering propagation rate and (d) blow-off limits.

Further increasing the external airflow velocity, the smoldering propagation rate eventually starts to decrease, where the cooling effect of external airflow (see Fig. 3b) on char-oxidation reaction at the

smoldering front can no longer be neglected. Then, the smoldering propagation rate is controlled by the competition between smoldering heat release and environmental cooling as

$$V_{sm} = \frac{\dot{q}''_{sm} - \dot{q}''_{loss}}{\rho_F c_F (T_{sm} - T_a)} = \frac{\rho_F \delta_T \dot{\omega}'''_{sm} \Delta H_{sm} - \dot{q}''_{loss}}{\rho_F c_F (T_{sm} - T_a)} \quad \text{(Chemical Regime)} \quad (5)$$

where $\dot{\omega}_{sm}$ and ΔH_{sm} are the rate and heat of smoldering reaction, respectively. Analogous to the flame spread [11,17], such a smoldering propagation is called the Chemical Regime [11]. Thus, as the airflow increases, the convective cooling ($\dot{q}''_{loss}$) increases to slow down the smoldering propagation. Eventually, the cooling rate of airflow may equal or exceed the heat release rate of smoldering ($\dot{q}''_{loss} \geq \dot{q}''_{sm}$), so the blow-off or the quenching by airflow occurs (discussed more in Section 3.4). Similar smoldering extinction behaviors were also observed in the quenching by the cold wall [29] and fuel moisture.

3.4. Smoldering blow-off limits

Table 1 and Fig. (4d, 5d) summarize the blow-off limits of both concurrent and opposed smoldering propagation over incenses with different fuel diameters and densities. Clearly, the blow-off of concurrent smoldering propagation is much more difficult than opposed smoldering propagation. For example, for 2.5-mm thick incense, the blow-off limits of concurrent and opposed smoldering propagation are 30 m/s and 14 m/s, respectively. As discussed in Section 3.2 and Fig. 3(b), compared to the smoldering propagation under concurrent airflow, the opposed airflow can directly attack the preheated zone, thus increasing cooling efficiency on the unburnt fuel. Therefore, smoldering propagation is easier to achieve blow-off under opposed airflow. Such a trend is also similar to the flame spread, where the blow-off of opposed flame spread can be achieved in a smaller wind speed [24].

On the other hand, as shown in Fig. 4(d), when the fuel density is 720 kg/m^3, as the fuel diameter increases from 1.5 mm to 5.0 mm, the blow-off airflow velocity (U_{ex}) of smoldering propagation decreases from 46 m/s to 24 m/s under the concurrent airflow and from 15 m/s and 13 m/s under the opposed airflow, respectively. Similarly, as shown in Fig. 5(d), the blow-off limits of both concurrent and opposed smoldering decrease as the fuel density increases from 720 kg/m^3 to 1,100 kg/m^3 with the same fuel diameter of 1.5 mm (see more analysis in Section 3.5 and 3.6).

More importantly, all the blow-off airflow velocities of smoldering (13-46 m/s) in the present work are higher than those of flame spread, for example, the concurrent flame spread over the thin wire (2 m/s) [41] and thin cellulose (~5.5 m/s) [48], or the opposed flame spread over PMMA rod (~3m/s) [24], thin paper/PMMA sheet (~1 m/s) [42] and thin cellulose (0.4-1 m/s) [43]. The observed blow-off airflow velocity of incense is also higher than 7 m/s of the opposed smoldering propagation over fiberboard [1]. Approximately, the blow-off airflow velocity of smoldering propagation is about one order of magnitude larger than that of flame spread, so that smoldering is much more persistent than flaming.

From Eq. (5), the blow-off or the quenching by airflow occurs (i.e., $V_{sm} = 0$) when the cooling rate of airflow equals to the heat release rate of smoldering as $\dot{q}''_{loss} = \dot{q}''_{sm}$, where the cooling flux at the

extinction limit could be further expressed as [46]

$$\dot{q}''_{loss} = h\left(T_{sm,min} - T_a\right) = C\left(\frac{U_{ex}d}{\upsilon}\right)^m \frac{\lambda_a}{d}\left(T_{sm,min} - T_a\right) \tag{6}$$

For simplicity, by assuming $m = 1$, we obtain

$$\dot{q}''_{sm} = \rho_F \delta_T \dot{\omega}'''_{sm} \Delta H_{sm} = \dot{q}''_{loss} = \left(\frac{CU_{ex}\lambda_a}{\upsilon}\right)\left(T_{sm,min} - T_a\right) \tag{7}$$

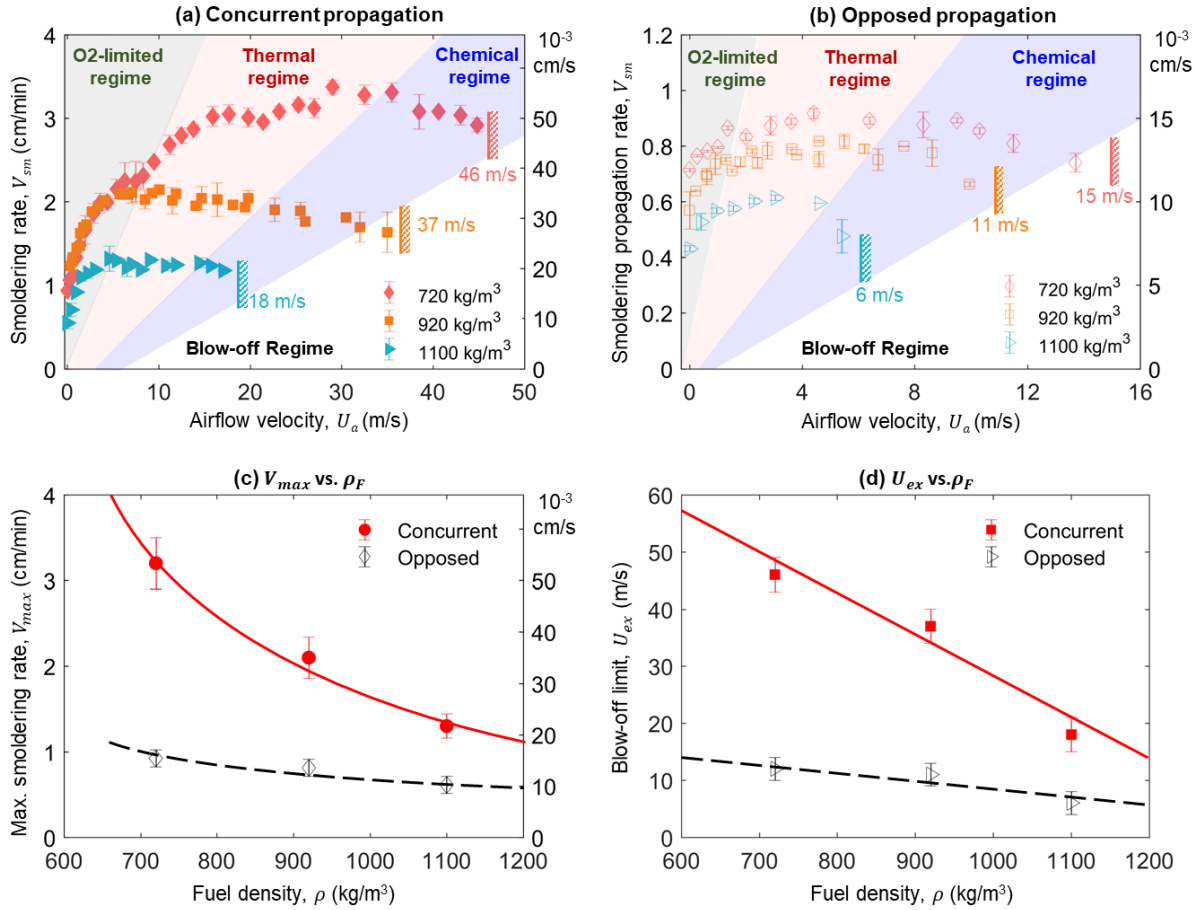

Fig. 5 Effect of fuel density on the rate of smoldering propagation under (a) concurrent and (b) opposed airflow, (c) maximum smoldering propagation rate, V_{max}, and (d) blow-off airflow velocity, U_{ex}.

To further evaluate the cooling effect of external flow, a smoldering Damkohler number (Da_{sm}) could be proposed referring to the Da of flame, as the ratio of the flow residence time scale (t_{fl}) to the reaction time scale (t_{ch}) [11] as

$$Da_{sm} = \frac{t_{fl}}{t_{ch}} = \frac{\frac{\delta_T}{U_{ex}}}{\frac{1}{\dot{\omega}'''_{sm}}} = \frac{\delta_T \dot{\omega}'''_{sm}}{U_{ex}} \tag{8}$$

Similar concept was also proposed for heterogenous combustion of carbon by Tsuji and Matsui [49]. At the blow-off limit, a critical smoldering Damkohler number can be defined from Eqs. (7,8) as

$$Da_{sm}^{*} = \frac{C\lambda_a\left(T_{sm,min} - T_a\right)}{\upsilon\rho_F \Delta H_{sm}} = \text{Const.} \quad (9)$$

which is essentially a constant depending on fuel properties and flow conditions, like the conventional critical Damkohler number for the blow-off limit of flame[9]. Note that as the fuel size and geometry changes, the flow field (C and m) will change, so that the value of Da_{sm}^{*} will change accordingly.

Table 1. The maximum smoldering propagation rate (V_{max}) and blow-off airflow velocity (U_{ex}) over incenses with different fuel diameters and densities.

Diameter d (mm)	Density ρ (kg/m^3)	Maximum smoldering rate, V_{max} (cm/min)		Blow-off limit, U_{ex} (m/s)	
		Concurrent	opposed	Concurrent	opposed
1.5	720	3.2	0.9	46	15
2.5	720	2.1	0.7	30	14
5.0	720	1.2	0.5	24	13
1.5	920	2.1	0.8	37	11
1.5	1,100	1.3	0.6	18	8

3.5. Effect of fuel diameter

Fig. 4(a-b) further compares the effect of fuel diameter (d) on smoldering propagation under external airflow. For both concurrent and opposed smoldering propagations, the propagation rate increases as the fuel diameter decreases. It is consistent with the trend of flame spread in the literature, i.e., a faster flame spread for a smaller-diameter fuel [28,50]. For example, under the airflow velocity of 5 m/s, as the fuel diameter increases from 1.5 mm to 5 mm, the concurrent smoldering propagation rate decreases from 2.1 cm/min to 1.1 cm/min, and the opposed smoldering propagation rate declines from 0.9 cm/min to 0.5 cm/min. Clearly, the maximum smoldering propagation rate also decreases with the fuel diameter, as further compared in Fig. 4(c). From Eqs. (2,3), the internal airflow velocity (u_a) inside the conical porous char is inversely correlated with fuel diameter (d), thus the rate of oxygen supply decreases as the fuel diameter increases. As a result, the rate of smoldering propagation decreases with the fuel diameter, agreeing with the experimental results in Fig. 4.

The concept of B number (i.e., Spalding mass transfer number) has been widely used to estimate the flaming burning rate of liquid droplet fuels and solids [51–53]. Compared to conventional gasification mass transfer driven by the flame sheet and heat conduction in the gas phase, the pyrolysis surface for smoldering is driven by the char-oxidation and heat conduction in the solid phase. Thus, the same concept can be adopted in describing smoldering burning (or propagation). For a cylindrical rod, the smoldering propagation is two-dimensional in axial and radial directions (see the top view of control volume in Fig. 6). Considering the smoldering propagation in the radial direction and the analogy with

flaming burning of droplet [13,52] or cylindrical rod [53], the burning flux ($\dot{m}''_F$) of incense can also be approximated as

$$\dot{m}''_F = C\frac{\lambda_F}{c_F d}\ln(1+B) \tag{10}$$

where C is a fitting correlation, and B is a constant for a given fuel. Thus, the smoldering rate in the axial direction is comparable to the observed smoldering rate in the radial direction as

$$V_{sm} \approx V_{sm,r} \approx \frac{\dot{m}''_F}{\rho} \approx \frac{\alpha_F}{d} \tag{11a}$$

which decreases with the fuel diameter [52], agreeing with the experimental results in Fig. 4(a-c). Because of the curvature effect, the conductive heat flux concentrates towards a smaller radius. A similar expression is also derived from Eq. (4), with the diameter as the thermal length ($\delta_T \approx d$) as

$$V_{sm} \approx \frac{\alpha_F}{\delta_T} \approx \frac{\alpha_F}{d} \tag{11b}$$

As seen from Fig. 2, the smoldering front thickness (δ_T) increases as the fuel diameter increases (d).

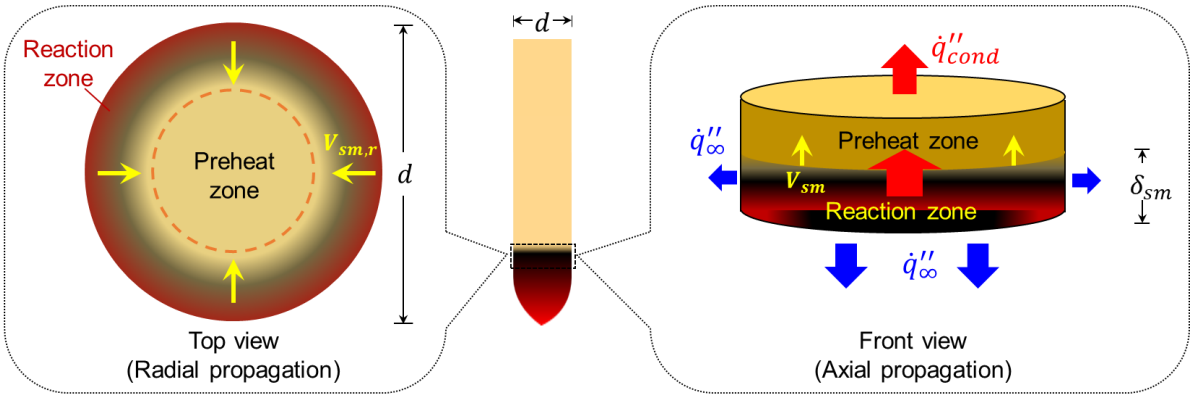

Fig. 6. Schematic diagram of the 2-D (radial and axial) smoldering propagation on a cylindrical fuel and the primary heat transfer processes.

On the other hand, as discussed in Section 3.4, the blow-off limit of smoldering was found to decrease as the fuel diameter increases (Fig. 4d). This trend is opposite to the flame spread, where the blow-off of a thinner fuel occurs at a smaller airflow velocity and the same critical strain rate ($a^* = U_{ex}/d$) [24,41]. Fundamentally, the concept of strain rate can be used for flame because the external wind can pull and bend the gaseous flame sheet. Nevertheless, the smoldering front in the solid phase cannot be bent like a flame sheet by the external flow. Therefore, the definition of critical strain rate for blow-off may not be applicable to smoldering combustion.

To explain the influence of fuel diameter on the smoldering blow-off limit (U_{ex}), a simplified energy conservation equation is applied to the near-limit reaction zone (see the front view of control volume in Fig. 6). At the blow-off extinction limit, the smoldering rate is zero; the reaction-zone

thickness is minimal ($\delta_{sm} \ll d$); and the bottom size is already quenched by the large wind. Then, the heat generation in the oxidation reaction zone is equal to the convective heat loss due to the airflow ($\dot{q}''_{\infty}$) and the conduction to the preheat zone ($\dot{q}''_{cond}$) as

$$(\pi d\delta_{sm})\dot{m}''_{O_2,max}\Delta H_{ox} = (\pi d^2)(T_{sm} - T_a)\left(h + \frac{\lambda_F}{\delta_{sm}}\right) \tag{12}$$

where the convective heat loss from the side for the thin oxidation zone is neglected, and the oxidation rate from the side has reached a maximum ($\dot{m}''_{O_2,max}$) and can no longer increase with airflow.

Then, the required convective cooling coefficient (h) can be derived, which also increases with the increased airflow velocity and the decreased fuel diameter, as

$$h = \frac{C_{sm}}{d} - \frac{\lambda_F}{\delta_{sm}} = Nu\frac{\lambda_a}{d} \propto \left(\frac{U_{ex}}{d}\right)^m \tag{13}$$

where $C_{sm} = \delta_{sm}\dot{m}''_{O_2,max}\Delta H_{ox}/(T_{sm} - T_a)$ is a smoldering constant, and $m = 1$ is assumed for simplicity. Thus, by rearranging Eq. (13), the dependence of blow-off airflow velocity with fuel diameter can be expressed as

$$U_{ex} \propto C_{sm} - d\frac{\lambda_F}{\delta_{sm}} \tag{14}$$

Therefore, as the fuel diameter (d) increases, the required external airflow velocity to blow off smoldering fire decreases, agreeing with experimental results in Fig. 4(d). Note that if the fuel diameter further decreases below 1 mm (i.e., an ultra-thin fuel), the strong wind may easily break and remove the smoldering zone. Then, the extinction is no longer a blow-off but a fuel-removal, which needs further experimental verification.

3.6. Effect of fuel density

Fig. 5(a-b) also shows the effect of fuel (bulk) density on the concurrent and opposed smoldering propagation rate, where the maximum rate of smoldering propagation was further compared in Fig. 5c. As expected, as the fuel density decreases, the smoldering propagation rate increases, agreeing with the theoretical analysis of Eqs. (1,2) where the maximum propagation rate is inversely proportional to the fuel density ($V_{sm} \propto 1/\rho_F$). For example, as the fuel density increases from 720 to 1,100 kg/m^3 under the wind velocity of 10 m/s, the smoldering propagation rate decreases from 2.1 cm/min to 1.3 cm/min for the concurrent spread and from 0.9 cm/min to 0.5 cm/min for the opposed spread, respectively.

As the (bulk) fuel density of porous media increases ($\rho_F = (1-\phi)\rho_s$), its porosity and permeability decrease. Thus, at the blow-off limit, the maximum airflow into the porous fuel ($\dot{m}''_{O_2,max}$) decreases, which reduces the value of C_{sm} in Eq. (14). Moreover, the thermal conductivity of fuel increases with the density ($\lambda_F \propto \rho_F$), so that the radial heat conduction from the reaction zone to the preheat zone also increases. From Eq. (14), we can see the required blow-off airflow velocity (U_{ex}) decreases as the fuel density increases, agreeing with the experimental results in Fig. 5(d).

4. Conclusions

In this work, we use experimental approaches to investigate the smoldering propagation and blow-off over cylindrical incenses under concurrent and opposed external wind up to 50 m/s. There are no experimental data on the smoldering propagation at large wind speeds over 10 m/s and the blow-off limits of persistent smoldering fire before this study. For concurrent smoldering propagation, partial airflow may permeate into the porous glowing zone in the form of a Darcy flow, while the oxygen can only reach the char surface via diffusion for opposed smoldering propagation. Also, the conical glowing zone may preheat the concurrent airflow boundary layer to preheat the downstream unburnt fuel, which further promotes the concurrent smoldering propagation faster than the opposed propagation.

We also found that the smoldering propagation rate is very sensitive to the airflow rate. As external airflow velocity increases, the smoldering propagation rate first increases (O_2-limited Regime), and then remains stable at its maximum value for a wide range of airflow velocity (Thermal Regime). Afterwards, it slightly decreases (Chemical Regime) until blow-off. Comparatively, the flame-spread rate increases with the wind speed due to increased convective heating rather than increased oxygen supply. This is a significant difference between smoldering and flaming spread, because smoldering combustion is controlled by both oxygen supply and heat loss.

We report for the first time that the blow-off airflow velocity of smoldering propagation (13~46 m/s) is around one order of magnitude larger than that of flame spread, and it decreases as the fuel diameter or density increases. Blowing-off concurrent smoldering propagation is also more difficult than opposed propagation, similar to the blow-off of flame spread. Future numerical simulations are needed to reveal the underlying physical and chemical process of smoldering propagation and blow-off under different airflow velocities.

CRediT authorship contribution statement

Shaorun Lin: Investigation, Writing-original draft, Formal analysis, Resources. **Tsz Him Chow:** Investigation, Resources. **Xinyan Huang:** Conceptualization, Supervision, Writing-review & editing, Funding acquisition.

Declaration of competing interest

The authors declare no conflicts of interest.

Acknowledgments

This research is funded by the National Natural Science Foundation of China (NSFC) No. 51876183 and the Society of Fire Protection Engineers (SFPE) Educational & Scientific Foundation. The authors thank Dr. Supan Wang (Nanjing Tech Univ.) for helping conduct thermal analysis of the incense sample. The comments from Dr. Han Yuan (Hong Kong PolyU) are also acknowledged.

References

[1] Palmer KN. Smouldering combustion in dusts and fibrous materials. *Combustion and Flame* 1957;1:129–54.

[2] Rein G. Smoldering Combustion. *SFPE Handbook of Fire Protection Engineering* 2014;2014:581–603.

[3] Ohlemiller TJ. Modeling of smoldering combustion propagation. *Progress in Energy and Combustion Science* 1985;11:277–310.

[4] Torero JL, Gerhard JI, Martins MF, Zanoni MAB, Rashwan TL, Brown JK. Processes defining smouldering combustion: Integrated review and synthesis. *Progress in Energy and Combustion Science* 2020;81:100869.

[5] Restuccia F, Ptak N, Rein G. Self-heating behavior and ignition of shale rock. *Combustion and Flame* 2017;176:213–9.

[6] Koya L, Gard C. Investigating the Attacks on the World Trade Center. First edit. New York: The Rosen Publishing Group, Inc.; 2018.

[7] Rein G. Smouldering Fires and Natural Fuels. In: Claire M. Belcher, editor. Fire Phenomena in the Earth System, New York: John Wiley & Sons, Ltd.; 2013, p. 15–34.

[8] Song Z, Huang X, Kuenzer C, Zhu H, Jiang J, Pan X, et al. Chimney effect induced by smoldering fire in a U-shaped porous channel: A governing mechanism of the persistent underground coal fires. *Process Safety and Environmental Protection* 2020;136:136–47.

[9] Williams FA. Mechanisms of fire spread. *Symposium (International) on Combustion* 1977;16:1281–94.

[10] Gollner MJ, Miller CH, Tang W, Singh A V. The effect of flow and geometry on concurrent flame spread. *Fire Safety Journal* 2017;91:68–78.

[11] Huang X, Gao J. A review of near-limit opposed fire spread. *Fire Safety Journal* 2021;120:103141.

[12] Fernandez-Pello AC, Hirano T. Controlling mechanisms of flame spread. *Combustion Science and Technology* 1983;32:1–31.

[13] Quintiere JG. Fundamentals of fire phenomena. John Wiley; 2006.

[14] Fernandez-Pello a. C, Ray SR, Glassman I. Downward Flame Spread In an Opposed Forced Flow. *Combustion Science and Technology* 1978;19:19–30.

[15] Xie Q, Zhang Z, Lin S, Qu Y, Huang X. Smoldering Fire of High-Density Cotton Bale Under Concurrent Wind. *Fire Technology* 2020;56:2241–56.

[16] Huang X, Restuccia F, Gramola M, Rein G. Experimental study of the formation and collapse of an overhang in the lateral spread of smouldering peat fires. *Combustion and Flame* 2016;168:393–402.

[17] Kumar A, Shih HY, T'ien JS. A comparison of extinction limits and spreading rates in opposed and concurrent spreading flames over thin solids. *Combustion and Flame* 2003;132:667–77.

[18] Konno Y, Hashimoto N, Fujita O. Downward flame spreading over electric wire under various oxygen concentrations. *Proceedings of the Combustion Institute* 2019;37:3817–24.

[19] Kadowaki O, Suzuki M, Kuwana K, Nakamura Y, Kushida G. Limit conditions of smoldering spread in counterflow configuration: Extinction and smoldering-to-flaming transition. *Proceedings of the Combustion Institute* 2020;000:1–9.

[20] Yamazaki T, Matsuoka T, Nakamura Y. Near-extinction behavior of smoldering combustion under highly vacuumed environment. *Proceedings of the Combustion Institute* 2019;37:4083–90.

[21] Sato J, Sato K, Hirano T. Fire spread mechanisms along steel cylinders in high pressure oxygen. *Combustion and Flame* 1983;51:279–87.

[22] Yamazaki T, Matsuoka T, Nakamura Y. Near-extinction behavior of smoldering combustion under highly vacuumed environment. *Proceedings of the Combustion Institute* 2019;37:4083–90.

[23] Lin S, Liu Y, Huang X. Climate-induced Arctic-boreal peatland fire and carbon loss in the 21st century. *Science of the Total Environment* 2021;796:148924.

[24] Huang X, Link S, Rodriguez A, Thomsen M, Olson S, Ferkul P, et al. Transition from opposed flame spread to fuel regression and blow off: Effect of flow, atmosphere, and microgravity. *Proceedings of the Combustion Institute* 2019;37:4117–26.

[25] Gollner MJ, Williams F., Rangwala A. Upward flame spread over corrugated cardboard. *Combustion and Flame* 2011;158:1404–12.

[26] Huang X, Rein G. Downward Spread of Smoldering Peat Fire: the Role of Moisture, Density and Oxygen Supply. *International Journal of Wildland Fire* 2017;26:907–18.

[27] Zhou Y, Gong J, Jiang L, Chen C. Orientation effect on upward flame propagation over rigid polyurethane foam. *International Journal of Thermal Sciences* 2018;132:86–95.

[28] Jiang L, He JJ, Sun JH. Sample width and thickness effects on upward flame spread over PMMA surface. *Journal of Hazardous Materials* 2018;342:114–20.

[29] Lin S, Huang X. Quenching of smoldering: Effect of wall cooling on extinction. *Proceedings of the Combustion Institute* 2021;38:5015–22.

[30] Fernandez-Pello AC. Flame Spread Modeling. *Combustion Science and Technology* 1984;39:119–34.

[31] Torero JL, Fernandez-Pello AC, KitanO M. Opposed forced flow smoldering of polyurethane foam. *Combustion Science and Technology* 1993;91:95–117.

[32] Kuwana K, Suzuki K, Tada Y, Kushida G. Effective Lewis number of smoldering spread over a thin solid in a narrow channel. *Proceedings of the Combustion Institute* 2017;36:3203–10.

[33] Valdivieso JP, Rivera J de D. Effect of Wind on Smoldering Combustion Limits of Moist Pine Needle Beds. *Fire Technology* 2014;50:1589–605.

[34] Santoso MA, Christensen EG, Yang J, Rein G. Review of the Transition From Smouldering to Flaming Combustion in Wildfires. *Frontiers in Mechanical Engineering* 2019;5.

[35] He M, Ding L, Yu L, Ji J. Effect of density on the smoldering characteristics of cotton bales ignited internally. *Proceedings of the Combustion Institute* 2020;000:1–9.

[36] Wang S, Huang X, Chen H, Liu N. Interaction between flaming and smouldering in hot-particle ignition of forest fuels and effects of moisture and wind. *International Journal of Wildland Fire* 2017;26:71–81.

[37] Bar-Ilan A, Putzeys OM, Rein G, Fernandez-Pello AC, Urban DL. Transition from forward smoldering to flaming in small polyurethane foam samples. *Proceedings of the Combustion Institute* 2005;30:2295–302.

[38] Emberley R, Inghelbrecht A, Yu Z, Torero JL. Self-extinction of timber. *Proceedings of the*

Combustion Institute 2017;36:3055–62.

[39] Dosanjh SS, Pagni PJ, Fernandez-Pello AC. Forced cocurrent smoldering combustion. *Combustion and Flame* 1987;68:131–42.

[40] Loh HT, Fernandez-Pello AC. Flow Assisted Flame Spread Over Thermally Thin Fuels. *Western States Section, Combustion Institute (Paper)* 1984:65–74.

[41] Lu Y, Huang X, Hu L, Fernandez-Pello C. Concurrent Flame Spread and Blow-Off Over Horizontal Thin Electrical Wires. *Fire Technology* 2019;55:193–209.

[42] Fernandez-Pello AC, Ray SR, Glassman I. Flame spread in an opposed forced flow: the effect of ambient oxygen concentration. *Symposium (International) on Combustion* 1981;18:579–89.

[43] Carmignani L, Celniker G, Bhattacharjee S. The Effect of Boundary Layer on Blow-Off Extinction in Opposed-Flow Flame Spread over Thin Cellulose: Experiments and a Simplified Analysis. *Fire Technology* 2017;53:967–82.

[44] Leach S V, Ellzey JL, Ezekoye OA. Convection , Pyrolysis , and Damko Extinction of Reverse Smoldering Combustion. *Twenty-Seventh Symposium (International) on Combustion* 1998:2873–80.

[45] Yamazaki T, Matsuoka T, Li Y, Nakamura Y. Applicability of a Low-Pressure Environment to Investigate Smoldering Behavior Under Microgravity. *Fire Technology* 2020.

[46] Incropera FP. Principles of heat and mass transfer. John Wiley; 2007.

[47] De Ris JN. Spread of a laminar diffusion flame. *Symposium (International) on Combustion* 1969;12:241–52.

[48] Wang S, Wang S, Zhu K, Xiao Y, Lu Z. Near Quenching Limit Instabilities of Concurrent Flame Spread over Thin Solid Fuel. *Combustion Science and Technology* 2016;188:451–71.

[49] Tsuji H, Matsui K. An aerothermochemical analysis of combustion of carbon in the stagnation flow. *Combustion and Flame* 1976;26:283–97.

[50] Ayani MB, Esfahani JA, Mehrabian R. Downward flame spread over PMMA sheets in quiescent air: Experimental and theoretical studies. *Fire Safety Journal* 2006;41:164–9.

[51] Rich D, Lautenberger C, Torero JL, Quintiere JG, Fernandez-Pello C. Mass flux of combustible solids at piloted ignition. *Proceedings of the Combustion Institute* 2007;31 II:2653–60.

[52] Kanury AM. Rate of charring combustion in a fire. *Symposium (International) on Combustion* 1973;14:1131–42.

[53] Lee CK. Burning rate of fuel cylinders. *Combustion and Flame* 1978;32:271–6.

Appendix

The incense sample was firstly pulverized into powders for TGA-DSC tests. The initial mass of peat was about 5 mg, and samples were heated at the constant rates of 10 K/min. Two oxygen concentrations were selected, 0% (nitrogen) and 21% (air). Experiments were repeated twice for each case, and good repeatability is shown. Fig. A1 shows the mass-loss rate (DTG) and heat flow (DSC) curves, respectively. Regardless of the oxygen concentration, the mass-loss rate rapidly increases at around 250°C, which can be defined as the pyrolysis temperature. The heat of smoldering (ΔH_{sm}) can be calculated by integrating the heat flow curve, and it is about 18 MJ/kg for this incense.

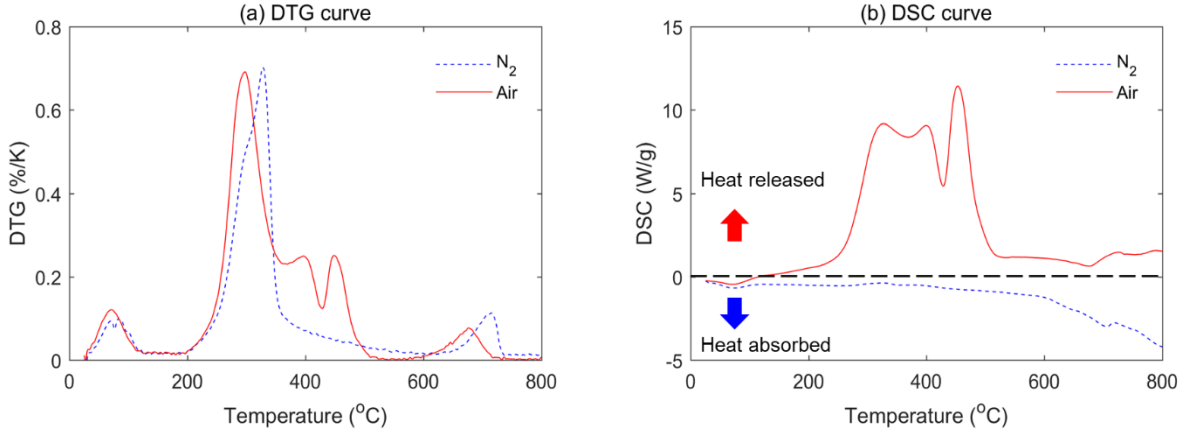

Fig. A1 TGA-DSC results of incense sample under air and nitrogen flow at a heating rate of 10 K/min, (a) normalized mass loss rate; and (b) heat flow as a function of temperature.

Fig. A2 shows some examples of required duration (t) for a reaction front to propagate through a certain distance of Δx under different airflow directions and velocities. Good linearity between Δx and t indicates the steady-state of smoldering fire propagation, where the slopes of the fitting lines are the corresponding smoldering propagation rates (V_{sm}).

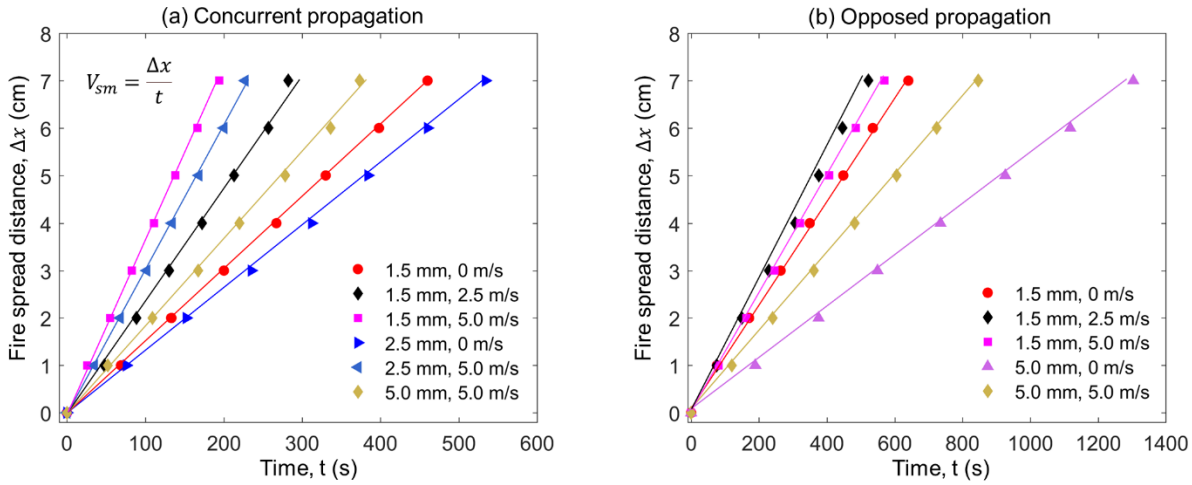

Fig. A2. Examples of smoldering front position (Δx) vs. the experimental duration (t) over the incense with different diameters under different airflow velocities.